Aggregation of $[Cu^{II}_4]$ Building Blocks into $[Cu^{II}_8]$ Clusters or a $[Cu^{II}_4]_\infty$ Chain through Subtle Chemical Control

Guillem Aromí,*[a] Joan Ribas,[a] Patrick Gamez,[b] Olivier Roubeau,[c] Huub Kooijman,[d] Anthony L. Spek,[d] Simon Teat,[e] Elizabeth MacLean,[e] Helen Stoeckli-Evans,[f] and Jan Reedijk[b]

Abstract: Coordination complexes of the ligand H_3L [1,3-bis(3-oxo-3-phenylpropionyl)-2-hydroxy-5-methylbenzene] with Cu^{II} are reported. Clusters showing various nuclearities or modes of supramolecular organization have been prepared by slightly changing the reaction conditions and have been crystallographically characterized. The reaction of H_3L with one equivalent of $Cu(OAc)_2$ in DMF yields the dinuclear complex $[Cu_2(HL)_2(dmf)_2]$ (**1**). Reaction in MeOH of H_3L with an increased amount of metal, in the form of $Cu(NO_3)_2$, and excess strong base (nBu$_4$NOH) affords the cluster $[Cu_8(L)_2(OMe)_8(NO_3)_2]$ (**2**). Complex **2** is a dimer of two linear $[Cu_4]$ arrays bridged by methoxide ligands, where the polynucleating ligand is fully deprotonated. The $[Cu_4]_2$ clusters are linked to each other by NO_3^- bridges to form one-dimensional coordination polymers. The link between $[Cu_8]$ units and their relative spatial positioning can be modified by changing the anion of the Cu^{II} salt, as demonstrated by the synthesis of the cluster polymers $[Cu_8(L)_2(OMe)_8Cl_2]$ (**3**) and $[Cu_8(L)(OMe)_{7.86}Br_{2.14}]$ (**4**), where only NO_3^- has been replaced by Cl^- or Br^-, respectively. Similarly, when ClO_4^- is used, compound $[Cu_8(L)_2(OMe)_8(ClO_4)_2(MeOH)_4]$ (**5**) can be isolated. It contains independent $[Cu_8]$ units. A slight change in the stoichiometry of the reaction leading to **2** affords the related complex *catena*-$[Cu_4(L)(OMe)_3(NO_3)_2(H_2O)_{0.36}]$ (**6**). This polymer contains essentially the same $[Cu_4]$ moiety as **2**, albeit organized in a completely different arrangement. Each $[Cu_4]$ unit in **6** is linked by OMe^- ligands to two such equivalent groups to form an infinite chain. Magnetic susceptibility measurements reveal weak antiferromagnetic exchange between Cu^{II} centers in **1** ($J = -0.73\ cm^{-1}$) and strong antiferromagnetic coupling within $[Cu_4]$ chains in **2**, **5**, and **6** (most negative J values of -113.8 and $-177.3\ cm^{-1}$ for **2** and **6**, respectively).

Keywords: beta-diketones · coordination polymers · copper · ligand design · magnetic properties

Introduction

An essential element of the spectacular progress experienced in the area of molecular magnetism during the last decade has been the creation of its objects of study. An illustration of this is the discovery of the phenomenon called single-molecule magnetism by which individual molecules can retain the orientation of their magnetic moment below a certain temperature.[1–3] The preparation of a handful of molecular compounds presenting this fascinating behavior (single-molecule magnets, SMMs)[4–6] has preceded much of the work that is leading to the understanding of the conditions and physicochemical properties that are necessary to observe it.[7,8] A great synthetic effort is still essential for the production of systems that will allow better understanding and control of the new properties observed, and eventually to discover new phenomena. Therefore, a major goal in this respect continues to be the preparation of multinuclear transition-metal complexes with unprecedented topologies, capable of presenting new and interesting magnetic properties. After many years devoted to this aim by a variety of groups, it has been recognized that the large number of synthetic

[a] Dr G. Aromí, Prof. Dr J. Ribas
Departament de Química Inorgànica, Universitat de Barcelona
Diagonal 647, 08028 Barcelona (Spain)
Fax: (+34) 93-490-7725
E-mail: guillem.aromi@qi.ub.es

[b] Dr P. Gamez, Prof. Dr J. Reedijk
Leiden Institute of Chemistry
Gorlaeus Laboratories, Leiden University
PO Box 9502, 2300 RA Leiden (The Netherlands)

[c] Dr O. Roubeau
Centre de Recherche Paul Pascal-CNRS UPR8641
115 avenue du Dr Schweitzer, 33600 Pessac (France)

[d] Dr H. Kooijman, Prof. Dr A. L. Spek
Bijvoet Center for Biomolecular Research
Crystal and Structural Chemistry, Utrecht University
Padualaan 8, 3584 CH Utrecht (The Netherlands)

[e] Dr S. Teat, Dr E. MacLean
CCLRC Daresbury Laboratory
Daresbury, Warrington, Cheshire, WA4 4AD (UK)

[f] Prof. Dr H. Stoeckli-Evans
Laboratoire de Cristallographie, Institut de Chimie
Université de Neuchâtel
Av. de Bellevaux 51, C.P. 2, 2007 Neuchâtel (Switzerland)

Supporting information for this article is available on the WWW under http://www.chemeurj.org or from the author.

DOI: 10.1002/chem.200400671

methodologies employed can be located anywhere within a spectrum delimited by two contrasting approaches. These two opposing strategies have been termed "serendipitous approach" and "molecular rational design", respectively. The first method relies on the high versatility of certain bridging ligands to stabilize transition-metal aggregates with a variety of geometries.[9] The precise structure of the ensuing clusters can be determined by many factors. It is therefore extremely difficult to predict and most often the explanation is given after the fact. The second method allows the synthesis of polynuclear complexes with a previously designed structure. This is possible when precise knowledge is available about the manner in which the various components of the reaction system are going to assemble.[10,11] In this context, the design and preparation of polynucleating ligands with a complex structure, which is capable of directing the aggregation of various metals in a precise topology, has led to the preparation of aggregates in a variety of impressive architectures.

Abstract in Catalan: *Diversos complexos de coordinació del lligand H_3L (1,3-bis(3-oxo-3-fenilpropionil)-2-hidroxi-5-metilbenzè) amb Cu^{II} són presentats. S'han preparat clústers que mostren una gran varietat de nuclearitats i modes d'organització supramolecular, només canviant lleugerament les condicions de reacció, els quals han estat caracteritzats cristal·logràficament. La mescla de H_3L amb un equivalent de $Cu(AcO)_2$ en DMF proporciona el complex dinuclear $[Cu_2(HL)_2(dmf)_2]$ (**1**). La reacció en MeOH de H_3L amb una major quantitat de metall en forma de $Cu(NO_3)_2$ i un excés d'una base forta (nBu_4NOH) dóna lloc al clúster $[Cu_8(L)_2(OMe)_8(NO_3)_2]$ (**2**). El complex **2** és un dímer de dues sèries lineals $[Cu_4]$ enllaçades per ponts metòxid, on el lligand polinucleant es troba completament desprotonat. Els clústers $[Cu_4]_2$ estan units entre ells mitjançant ponts NO_3^-, tot formant polímers de coordinació uni-dimensionals. La unió entre unitats $[Cu_8]$ i la seva disposició relativa en l'espai poden ésser modificades tot canviant l'anió de la sal de Cu^{II}, tal com queda demostrat amb la síntesi dels clústers polimèrics $[Cu_8(L)_2(OMe)_8Cl_2]$ (**3**) i $[Cu_8(L)_2(OMe)_{7.86}Cl_{2.14}]$ (**4**), on únicament s'ha canviat NO_3^- per Cl^- o Br^-, respectivament. De manera similar, quan s'utilitza ClO_4^- s'obté el compost $[Cu_8(L)_2(OMe)_8(ClO_4)_2(MeOH)_4]$ (**5**), format per unitats $[Cu_8]$ independents. Un petit canvi en l'estequiometria de la reacció que produeix el producte **2** dóna lloc al compost relacionat catena-$[Cu_4(L)(OMe)_3(NO_3)_2(H_2O)_{0.36}]$ (**6**). Aquest polímer conté essencialment la mateixa unitat $[Cu_4]$ del compost **2**, tot i que organitzada d'una manera completament diferent. Cada unitat $[Cu_4]$ en el compost **6** està unida per lligands MeO^- a dues unitats equivalents a ella mateixa, tot formant cadenes infinites. Mesures de susceptibilitat magnètica revelen intercanvi antiferromagnètic feble entre centres Cu^{II} en el compost **1** ($J = -0.73\ cm^{-1}$) i acoblament antiferromagnetic fort dins de les cadenes $[Cu_4]$ en els compostos **2**, **5** i **6** (amb màxims valors negatius de J de -113.8 i $-177.3\ cm^{-1}$ per a **2** i **6**, respectivament).*

In recent years, some of us have been exploring the coordination chemistry of a phenol-bis(β-diketonate) ligand[12] (H_3L, see Scheme 1), which was designed for the assembly

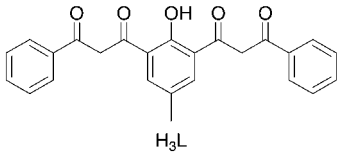

Scheme 1. The H_3L ligand.

of rows of closely spaced transition metals. Such an arrangement of 3d metals is of particular interest in the study of magnetic interactions within molecular magnets, and remarkable success has been achieved in this direction with polydentate *N*-ligands.[13–15] The new ligand H_3L possesses three ionizable protons that can be removed gradually and this has allowed the preparation of a variety of complexes with different metals featuring various nuclearities.[16–20] These complexes contain the ligand in its di- or trianionic form, depending on the amount of basic equivalents used in the reaction system. When only two protons are removed, the ligand was shown to be capable of assembling two or three metals within a molecular complex. Thus, the compounds with formulae $[Cu_2(HL)_2(dmf)_2]$ (**1**),[20] $[M_2(HL)_2(py)_4]$ (M^{II} = Ni^{II}, Mn^{II}, Co^{II}),[18] and $[Mn_3(HL)_3]$ have been prepared and characterized. If the three ionizable protons from H_3L are removed with an excess of base, the resulting ligand binds to a larger number of metal atoms, as demonstrated by the preparation of $[Cu_8(L)_2(OMe)_8(NO_3)_2]$ (**2**).[17] The later complex consists of two rows of four Cu^{II} ions held together by two L^{3-} ligands respectively, and linked to each other by bridging OMe^- groups to give octanuclear clusters. These $[Cu_8]$ moieties are organized in the solid state in the form of one-dimensional (1D) chains of clusters as a result of the bridging action of NO_3^- ligands. Herein we present full details of the structure of **2** and its magnetic properties. The association of $[Cu_8]$ units in the crystal has been modified by changing the nature of the counterion in the Cu^{II} salt. Thus, the synthesis and structure of the new Cl^-- and Br^--bridged coordination polymers $[Cu_8(L)_2(OMe)_8Cl_2]$ (**3**) and $[Cu_8(L)_2(OMe)_{7.86}Br_{2.14}]$ (**4**), respectively, are presented here. Likewise, with the preparation of the new complex $[Cu_8(L)_2(OMe)_8(ClO_4)_2(MeOH)_4]$ (**5**), it is shown in this report that the basic $[Cu_8]$ moieties can also exist as discrete clusters in the solid state. Finally, we report the preparation, structure, and magnetochemistry of a related compound, *catena*-$[Cu_4(L)(OMe)_3(NO_3)_2(H_2O)_{0.36}]$ (**6**), also containing $[Cu_4L]^{5+}$ moieties, but organized in a drastically different manner compared to **2**. The coordination polymer **6** was obtained by simply changing the amount of base used in the reaction system. Preliminary accounts of this work have been previously communicated.[17,20]

Results and Discussion

Synthesis: In previous work, we have shown the feasibility of selectively removing only two of the three acidic protons from the H_3L ligand by the use of a stoichiometric amount of a mild base. Thus, the dinuclear complexes $[M_2(HL)_2(py)_4]$ ($M = Mn^{II}$, Ni^{II}, Co^{II})[18] were prepared and characterized crystallographically, as well as the trinuclear molecule $[Mn_3(HL)_3]$.[16] Whether the latter or the dinuclear complex $[M_2(HL)_2(py)_4]$ is formed depends only on the presence or absence of pyridine in the system.[19] In all these compounds, both protons are provided by the β-diketone units, while the phenol moiety remains in its neutral form. Interestingly, a comparison of the Mn^{II} complex with the Ni^{II}/Co^{II} dinuclear analogues showed that the bis(diketonate) ligand displayed a completely different conformation depending on the preferred local *cis* versus *trans* configuration at the metal centers. The Co^{II} and Ni^{II} ions show a preference for the *trans* configuration of the py solvate ligands, leading to a *syn*,*syn* conformation of HL^{2-} in the assembly, whereas Mn^{II} displays the *cis* arrangement, leading to an architecture in which the ligand HL^{2-} adopts the *syn*,*anti* form.

Given the versatility in the coordination geometry of copper(II), it was of interest to study its behavior with respect to H_3L. The reaction of equimolar amounts of $Cu(AcO)_2$ and H_3L in DMF produced crystals of $[Cu_2(HL)_2(dmf)_2]$ (**1**) in 47% yield within a few hours of standing at −5 °C, according to the reaction in Equation (1).

$$2\,Cu(AcO)_2 + 2\,H_3L + 2\,DMF \rightarrow [Cu_2(HL)_2(dmf)_2] + 4\,AcOH \quad (1)$$

In this dimer, the Cu^{II} ions have a square-pyramidal coordination geometry (see Figure 1) and the HL^{2-} ligands are again in the *syn*,*syn* conformation, presumably allowing the most stable coordination geometry of Cu^{II} with the set of donors available in the system.

To extend the above results, the possibility was explored of generating a fully deprotonated form of H_3L as a potential way of binding a larger number of metals to this ligand. To this aim, the reaction of $Cu(NO_3)_2$ (1 mmol) and H_3L ($^1/_8$ mmol) in methanol was performed in the presence of an excess of a stronger base (1.8 mmol), namely nBu$_4$NOH. Recrystallization of the green solid that precipitated immediately led to the isolation of the new octanuclear complex $[Cu_8L_2(OMe)_8(NO_3)_2]$ (**2**). The crystal structure of this complex (see below) shows the L^{3-} form of the ligand chelating four Cu^{II} ions arranged in close proximity to each other in a metallic array, which was the goal that had prompted the preparation of H_3L originally. The $[Cu^{II}_4L]^{5+}$ oligomers dimerize into the octanuclear units of **2** as a result of the bridging action of the OMe^- groups, which are produced by the deprotonation of the solvent molecules by the remaining base. The large excess of MeOH in the system explains, in part, the fact that OMe^- ligands are found in the complex, rather than OH^- groups. Complex **2**, however, changes color from green to brown and loses crystallinity upon exposure to air. Microanalyses (see the Experimental Section) suggest that the compound undergoes complete hydrolysis in contact with atmospheric moisture. X-ray powder diffraction confirmed that the hydrolyzed product, **2a**, is composed of a different crystalline phase, as deduced by comparison of its diffraction pattern with that calculated from the single-crystal data of **2** (see Figure S1 in the Supporting Information). The solid-state structure of **2** (see below) also shows that the NO_3^- ligands serve as linkages that join the octanuclear aggregates to produce infinite linear cluster polymers. This observation prompted our interest in influencing the supramolecular organization of the $[Cu_8]$ units within the crystal by means of Cu^{II} salts of other anions. Thus the reaction above was repeated with $CuCl_2$ and $CuBr_2$ which led to the crystallization of the two new compounds $[Cu_8L_2(OMe)_8Cl_2]$ (**3**) and $[Cu_8(L)_2(OMe)_{7.86}Br_{2.14}]$ (**4**), respectively. Complexes **3** and **4** are very similar and feature the same $[Cu_8L_2]$ clusters as **2**, but linked by Cl^- or Br^- ions, respectively. In complex **4**, site occupancy disorder was found between μ-Br and μ-OMe, which explains the fractional numbers in the formula. The consequence of replacing NO_3^- by Cl^- or Br^- is essentially that of modifying the relative positions in the space of the octanuclear aggregates within the cluster polymer (see below). The possibility of using this method to further influence the spatial organization of the $[Cu_8L_2]$ units was explored by the use of $Cu(ClO_4)_2$ in the reaction. This led to the formation of the analogous complex $[Cu_8L_2(OMe)_8(ClO_4)_2(MeOH)_2]$ (**5**). It was found that the yield of this reaction improved significantly when the ratios between the reagents were adjusted in accordance with the composition of the final compound (see the Experimental Section). The crystal structure of this compound (see below) revealed the presence of isolated Cu_8 clusters in the crystals in which, this time, the ClO_4^- ions are each blocking two axial coordination positions of Cu^{II} but are not acting as a bridge between clusters. Structural data from complex **5** were originally collected on a conventional diffractometer that allowed the product to be identified; however, it gave a very bad fit owing to poor diffraction. Since this product was considered a key compound in this report, the data were collected again with a synchrotron radiation source, which provided an excellent data set (see below). Thus, in this manner, it was unequivocally demonstrated that the spatial positioning of the individual octanuclear units could be dramatically influenced by means of a small chemical variation.

As a different way to affect the structure of the final product, the reaction leading to **2** was performed with different stoichiometries. When a lower proportion of nBu$_4$NOH was used, more precisely, a 1:1:0.25 molar ratio of $Cu(NO_3)_2/n$Bu$_4$NOH/H_3L, no precipitate could be obtained from the mixture, which indicated that the reaction was following a different path. Upon addition of diethyl ether, crystals of a different compound, namely *catena*-$[Cu_4L(OMe)_3(NO_3)_2(H_2O)_{0.36}]$ (**6**), were obtained after leaving the system unperturbed for a few days. Coordination polymer **6** features $[Cu^{II}_4L]^{5+}$ oligomers as in **2**, again aggregated to each other by OMe^- bridges (see below). In complex **6**, however, each tetranuclear moiety is connected to two other identical

units to constitute the repeating step of an infinite one-dimensional ladder.

The above revelations underscore the feasibility of introducing small and subtle changes to a given reaction system to significantly change the supramolecular arrangement of a magnetic building block.

Description of structures: The structure of complex **1** has been reported with full details in a previous publication.[20] Only a brief description will be given here. Crystallographic details for complex **2** have been reported elsewhere.[17] Selected interatomic distances and bond angles of complexes **2** and **6** are given in Table 1 and Table 2, respectively. Average parameters are summarized for complexes **3**, **4**, and **5** in the captions to the figures.

Table 1. Selected interatomic distances [Å] and angles [°] for $[Cu_8(L)_2(OMe)_8(NO_3)_2]$ (**2**).[a]

Cu1–O5	1.922(3)	Cu1–O20b	1.958(3)	Cu1–O6	1.994(3)
Cu1–O18	1.954(3)	Cu1–O13a	2.226(3)	Cu2–O18	1.940(3)
Cu2–O6	1.963(3)	Cu2–O14b	1.935(2)	Cu2–O7	1.949(3)
Cu2–O16b	2.743(3)	Cu2–O11	2.340(3)	Cu3–O8	1.964(3)
Cu3–O14b	1.954(3)	Cu3–O12	2.433(3)	Cu3–O14	2.389(3)
Cu3–O7	1.953(3)	Cu3–O16	1.936(3)	Cu4–O20	1.921(3)
Cu4–O8	1.958(3)	Cu4–O18b	2.418(2)	Cu4–O9	1.906(3)
Cu4–O16	1.952(3)				
Cu1···Cu2	2.8999(8)	Cu2···Cu3	2.8834(7)	Cu3···Cu4	2.9995(8)
Cu1···Cu4b	2.9610(9)	Cu2···Cu4b	3.4677(8)	Cu2···Cu3b	3.3225(8)
Cu3···Cu3b	3.2981(8)	O5-Cu1-O6	90.73(12)	O5-Cu1-O20b	92.24(12)
O6-Cu1-O20b	140.11(11)	O13a-Cu1-O20b	100.67(12)	O5-Cu1-O18	170.23(12)
O6-Cu1-O18	81.27(11)	O18-Cu1-O13a	102.11(10)	O5-Cu1-O13a	86.66(12)
O6-Cu1-O13a	119.22(10)	O18-Cu1-O20b	90.37(11)	O6-Cu2-O18	82.43(11)
O7-Cu2-O11	96.00(10)	O7-Cu2-O16b	92.04(10)	O11-Cu2-O16b	168.16(9)
O14b-Cu2-O16b	80.01(10)	O6-Cu2-O7	89.47(11)	O6-Cu2-O14b	167.12(11)
O7-Cu2-O18	164.58(12)	O11-Cu2-O18	98.19(10)	O18-Cu2-O14b	102.36(11)
O6-Cu2-O11	98.86(10)	O6-Cu2-O16b	89.87(10)	O7-Cu2-O14b	82.99(11)
O11-Cu2-O14b	92.33(11)	O18-Cu2-O16b	74.92(10)	O7-Cu3-O14	85.37(10)
O8-Cu3-O12	96.51(11)	O8-Cu3-O14b	171.08(12)	O12-Cu3-O14b	86.74(10)
O16-Cu3-O14b	108.74(11)	O7-Cu3-O8	89.39(12)	O7-Cu3-O16	167.14(12)
O8-Cu3-O14	94.27(11)	O12-Cu3-O14	167.50(9)	O14-Cu3-O16	89.81(11)
O7-Cu3-O12	88.42(10)	O7-Cu3-O14b	82.38(11)	O8-Cu3-O16	79.08(12)
O12-Cu3-O16	98.43(11)	O14-Cu3-O14b	81.69(10)	O8-Cu4-O20	170.06(13)
O9-Cu4-O20	94.88(14)	O16-Cu4-O18b	83.06(11)	O8-Cu4-O9	91.55(14)
O8-Cu4-O18b	108.19(11)	O9-Cu4-O18b	96.49(12)	O20-Cu4-O18b	78.64(11)
O8-Cu4-O16	78.85(12)	O9-Cu4-O16	169.66(14)	O16-Cu4-O20	95.15(12)
Cu3-O14-Cu3b	98.31(10)	Cu2b-O14-Cu3b	95.68(12)	Cu3-O14-Cu2b	99.87(11)
Cu3-O16-Cu2b	88.75(10)	Cu3-O16-Cu4	100.96(13)	Cu4-O16-Cu2b	93.70(11)
Cu1-O18-Cu4b	84.55(10)	Cu1-O18-Cu2	96.27(12)	Cu2-O18-Cu4b	104.94(10)
Cu4-O20-Cu1b	99.50(13)	Cu1-O6-Cu2	94.24(12)	Cu2-O7-Cu3	95.28(12)
Cu3-O8-Cu4	99.75(13)	Cu1-Cu2-Cu3	159.78(2)	Cu2-Cu3-Cu4	170.18(3)

[a] Suffixes "a" and "b" denote symmetry operations $[1-x,-y,1-z]$ and $[2-x,-y,1-z]$, respectively.

*$[Cu_2(HL)_2(dmf)_2]$ (**1**)*: Complex **1** (Figure 1) is a centrosymmetric dinuclear complex containing two Cu^{II} ions in an almost square-pyramidal coordination environment ($\tau = 0.16$, where $\tau = 0$ or 1 for the perfect square-pyramidal and trigonal-bipyramidal geometries, respectively).[21] These two Cu^{II} ions are chelated and bridged by two HL^{2-} groups through their β-diketonate units. The apical position of each metal is occupied by one DMF solvent molecule, coordinated through its oxygen atom. The phenol moieties of the HL^{2-} ligand are not deprotonated and donate hydrogen bonds to O-acceptors from neighboring β-diketonate moieties.

*$[Cu_8(L)_2(OMe)_8(NO_3)_2]$ (**2**)*: Complex **2** (Figures 2–4) is a cluster of eight Cu^{II} centers arranged in two tetranuclear linear oligomers that are linked together by methoxide groups (six in the μ_3- and two in the μ-OMe^- mode). The asymmetric unit (Figure 2) contains four metals that have been gathered by the template action of one L^{3-} ligand, through the formation of four fused six-membered chelate rings involving a total of five oxygen donors. In these tetranuclear chains, the metals do not form a strictly linear array, as emphasized in Figure 4 (the Cu1-Cu2-Cu3 and Cu2-Cu3-Cu4 angles are 159.78(2)° and 170.18(3)°, respectively). The coordination around copper is completed by nitrate ligands in a very rare η^3:μ_3-NO_3^- binding mode,[22] which links each $[Cu_8L_2(OMe)_8]^{2+}$ aggregate to two other such fragments to result in the formation of a 1D coordination polymer of clusters (Figure 4). Of the four crystallographically independent Cu^{II} ions of **2**, two are in a distorted Jahn–Teller-elongated octahedral environment (Cu2 and Cu3), Cu1 is intermediate between trigonal bipyramidal and square pyramidal ($\tau = 0.50$), and Cu4 is in a square-pyramidal coordination geometry ($\tau = 0.01$). Of these coordination environments, the axial positions are taken by the six long bonds of the metal with μ_3-OMe^- groups, which connect both $[Cu_4]$ moieties to each other, or by the bonds with NO_3^- ligands. The Cu···Cu distances within the seven nonequivalent $[Cu_2O_2]$ pairs of the octanuclear aggregate (Figure 3 and Figure 12) are on average shorter within the tetranuclear arrays (2.8834(7) to 2.9995(8) Å) than between them (2.9610(9) to 3.4677(8) Å). The shortest intercluster Cu···Cu distance within the 1D chain is 5.2317(10) Å (Cu1···Cu2$[1-x,-y,1-z]$). A few coordination polymers of Cu^{II} clusters have been reported in the literature over the years, but the number of such species remains small.[22–25]

*$[Cu_8(L)_2(OMe)_8(Cl)_2]$ (**3**)*: Complex **3** (Figure 5) is structurally related to **2** in that it consists of almost identical octanuclear $[Cu_8L_2(OMe)_8]^{2+}$ aggregates linked by counterions. In **3**, the connection between clusters takes place with Cl^- ligands through coordination to copper with Cu-Cl-Cu angles of 127.28(6)°. The core of the $[Cu_8]$ units has essentially the same geometry as in **2**, except that two coordinating positions of Cu^{II} filled by NO_3^- in the previous complex are now vacant, the corresponding metals now presenting square-pyramidal geometry instead of octahedral (microanalysis shows these vacant positions to be occupied by H_2O molecules

Table 2. Selected interatomic distances [Å] and angles [°] for *catena*-$[Cu_4(L)(OMe)_3(NO_3)_2(H_2O)_{0.36}]$ (**6**).[a]

Cu1–O5	1.848(6)	Cu1–O6	1.947(3)	Cu1–O14	1.932(3)
Cu1–O1	2.413(15)	Cu1–O65	2.030(12)	Cu1–O11b	1.989(3)
Cu1–O14b	2.481(3)	Cu2–O6	1.928(3)	Cu2–O7	1.949(3)
Cu2–O11	2.410(3)	Cu2–O14	1.963(3)	Cu2–O16a	1.940(3)
Cu2–O21Aa	2.435(6)	Cu2–O21Ba	2.783(12)	Cu3–O7	1.953(3)
Cu3–O8	1.928(3)	Cu3–O12	2.676(4)	Cu3–O18	1.931(3)
Cu3–O16a	1.927(3)	Cu3–O18a	2.587(3)	Cu4–O8	1.952(3)
Cu4–O9	1.914(3)	Cu4–O16	2.367(3)	Cu4–O18	1.943(3)
Cu4–O21A	1.993(6)	Cu4–O22A	2.710(11)	Cu4–O21B	1.919(12)
Cu4–O22B	2.522(18)	Cu1···Cu2	2.9653(8)	Cu1···Cu1b	3.3255(8)
Cu1···Cu2b	3.3766(9)	Cu2···Cu3	2.8502(8)	Cu2···Cu4a	3.4294(8)
Cu3···Cu4	2.9945(8)	Cu3···Cu4a	3.2781(8)	Cu3···Cu3a	3.3097(8)
O5-Cu1-O6	93.0(2)	O5-Cu1-O14	172.8(2)	O5-Cu1-O11b	90.6(2)
O5-Cu1-O14b	99.7(2)	O6-Cu1-O14	80.24(12)	O6-Cu1-O1	93.8(4)
O6-Cu1-O65	87.7(4)	O6-Cu1-O11b	171.06(12)	O6-Cu1-O14b	91.56(11)
O14-Cu1-O1	87.3(4)	O14-Cu1-O65	165.0(4)	O14-Cu1-O11b	96.51(12)
O14-Cu1-O14b	83.00(11)	O1-Cu1-O65	84.6(5)	O1-Cu1-O11b	94.3(4)
O1-Cu1-O14b	167.9(3)	O65-Cu1-O11b	96.7(4)	O65-Cu1-O14b	106.5(4)
O11b-Cu1-O14b	79.75(11)	O6-Cu2-O7	89.58(12)	O6-Cu2-O11	88.36(11)
O6-Cu2-O14	79.94(12)	O6-Cu2-O16a	173.08(12)	O6-Cu2-O21Aa	101.46(17)
O6-Cu2-O21Ba	103.4(3)	O7-Cu2-O11	96.91(11)	O7-Cu2-O14	169.48(12)
O7-Cu2-O16a	83.78(12)	O7-Cu2-O21Aa	88.37(18)	O7-Cu2-O21Ba	93.0(3)
O11-Cu2-O14	82.09(11)	O11-Cu2-O16a	94.37(11)	O11-Cu2-O21Aa	168.92(15)
O11-Cu2-O21Ba	164.7(2)	O14-Cu2-O16a	106.72(12)	O14-Cu2-O21Aa	94.48(18)
O14-Cu2-O21Ba	90.2(3)	O16a-Cu2-O21Aa	76.46(17)		
O16a-Cu2-O21Ba	75.1(3)	O7-Cu3-O8	90.99(12)	O7-Cu3-O12	86.23(11)
O7-Cu3-O18	167.71(12)	O7-Cu3-O16a	84.03(12)	O7-Cu3-O18a	87.21(10)
O8-Cu3-O12	93.11(12)	O8-Cu3-O18	79.02(12)	O8-Cu3-O16a	174.90(12)
O8-Cu3-O18a	97.10(11)	O12-Cu3-O18	101.32(12)	O12-Cu3-O16a	87.66(11)
O12-Cu3-O18a	167.96(11)	O18-Cu3-O16a	105.78(12)	O18-Cu3-O18a	86.95(11)
O16a-Cu3-O18a	81.62(10)	O8-Cu4-O9	91.06(13)	O8-Cu4-O16	102.25(11)
O8-Cu4-O18	78.17(12)	O8-Cu4-O21A	173.2(2)	O8-Cu4-O22A	128.2(3)
O8-Cu4-O21B	171.2(4)	O8-Cu4-O22B	114.9(4)	O9-Cu4-O16	91.04(12)
O9-Cu4-O18	168.50(13)	O9-Cu4-O21A	95.7(2)	O9-Cu4-O22A	93.4(3)
O9-Cu4-O21B	88.1(4)	O9-Cu4-O22B	82.2(4)	O16-Cu4-O18	87.37(11)
O16-Cu4-O21A	77.19(18)	O16-Cu4-O22A	129.2(3)	O16-Cu4-O21B	86.5(4)
O16-Cu4-O22B	142.3(4)	O18-Cu4-O21A	95.0(2)	O18-Cu4-O22A	96.5(3)
O18-Cu4-O21B	103.1(4)	O18-Cu4-O22B	105.9(4)	O21A-Cu4-O22A	52.0(3)
O21B-Cu4-O22B	56.3(5)	Cu1-Cu2-Cu3	171.22(3)	Cu2-Cu3-Cu4	172.43(3)

[a] Labels A and B refer to major and minor components of the disordered structure, respectively, and suffixes "a" and "b" denote symmetry operations $[-x,1-y,-z]$ and $[1-x,1-y,-z]$, respectively.

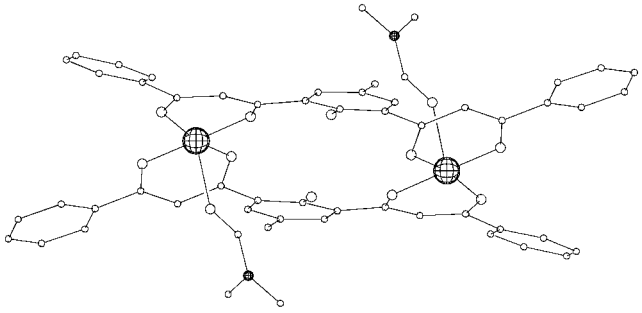

Figure 1. PLATON representation of $[Cu_2(HL)_2(dmf)_2]$ (**1**). Hydrogen atoms have been removed for clarity. Cu: large; O: medium; N: medium hashed spheres; C: rest.

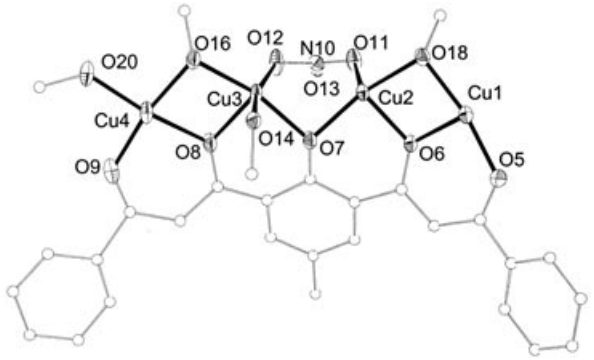

Figure 2. Representation of the asymmetric unit of $[Cu_8(L)_2(OMe)_8(NO_3)_2]$ (**2**). Hydrogen atoms have been removed for clarity. Non-carbon atoms are labeled and represented as displacement ellipsoids at the 50% probability level.

upon exposure to air). The distribution of coordination geometries within the asymmetric unit of **3** is thus one octahedral Cu^{II} ion with axial elongation (Cu3), two square-pyramidal (Cu2 and Cu4, with $\tau = 0.07$, and 0.06, respectively), and one ion in a geometry that is intermediate between square-pyramidal and trigonal-bipyramidal ($\tau = 0.54$). The Cu-Cu-Cu angles defining the bending of the metallic chain are 170.76(3)° (Cu1b-Cu3-Cu4c) and 155.65(3)° (Cu2c-Cu4c-Cu3), respectively. Ranges for selected interatomic distances and angles are listed in the caption to Figure 5. The main structural difference between **2** and **3**, as imposed by the replacement of Cl^- by NO_3^-, lies in the relative position of the $[Cu_8]$ clusters. The exchange of a tridentate bridge by a mononuclear link causes slippage of the clusters with respect to each other so that only two Cu ions per cluster participate in each intercluster link. This leads to shorter intercluster metal–metal distances (the shortest Cu···Cu vector, which corresponds to Cu1···Cu3, measures 4.473(2) Å). The Cu···Cu distances within $[Cu_2O_2]$ units are in the range 2.904(1) to 2.990(1) Å within the tetranuclear arrays and 3.013(2) to 3.567(2) Å across the chains, for both categories, only slightly longer than in **2**.

$[Cu_8(L)_2(OMe)_{7.86}(Br)_{2.14}]$ (***4***): Complex **4** (Figure 6) is almost the isostructural Br^- version of **3**. The chief difference with the latter is that the position occupied by μ-OMe^- is now partially filled with μ-Br^- with a site occupancy disorder that has a OMe^- to Br^- ratio of 93:7. This occupancy disorder explains the fractional numbers in the formula of **4**. The remaining features of this derivative are essentially the same as for the chloride compound, only

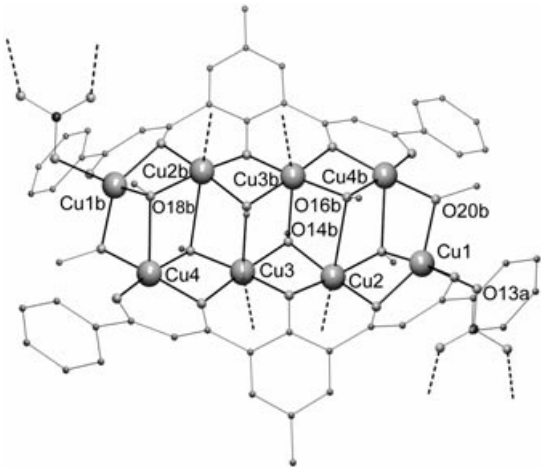

Figure 3. POV-Ray representation of the structure of $[Cu_8(L)_2(OMe)_8(NO_3)_2]$ (**2**) in the crystal. Cu atoms and atoms listed in Table 2 and not shown in Figure 2 are labeled. Hydrogen atoms have been removed for clarity. Cu: large gray; O: medium gray; N: medium black; C: rest. The dashed lines are bonds to neighboring homologous octanuclear units.

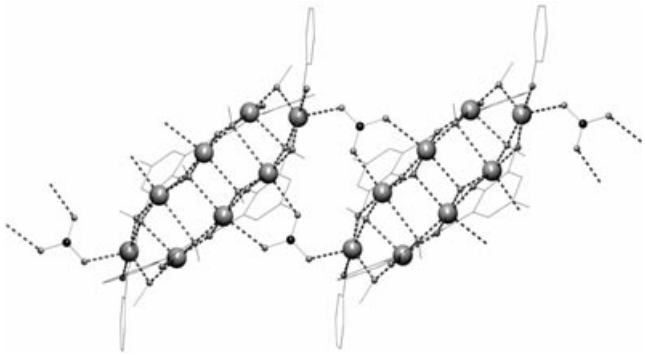

Figure 4. POV-Ray representation of $[Cu_8(L)_2(OMe)_8(NO_3)_2]$ (**2**) in the crystal emphasizing the polymerization of $[Cu_8]$ units into infinite 1D chains by η^3:μ_3-NO_3^- bridges. Hydrogen atoms have been removed for clarity. Cu: large gray; O: medium gray; N: medium black; C: rest. Bonds to Cu are highlighted as dashed lines.

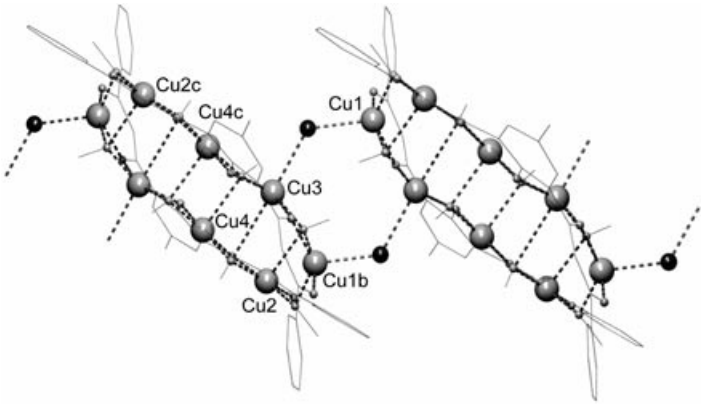

Figure 5. POV-Ray representation of the solid-state polymeric 1-D structure of $[Cu_8(L)_2(OMe)_8(Cl)_2]$ (**3**), achieved through the bridging of $[Cu_8]$ units by μ-Cl^- ions. Hydrogen atoms have been removed for clarity. The four independent Cu atoms, and these quoted in the text are labeled. Cu: large gray; O: small gray; Cl: medium black; C: rest. Bonds to Cu are highlighted as dashed lines. Bond length ranges [Å]: Cu–$O_{eq.}$ 1.904(4)–1.992(3); Cu–$O_{ax.}$ 2.385(3)–2.889(3); Cu–Cl 2.4208(17) and 2.5708(17); Cu1a–O2 2.022(3) (this bond is neither axial nor equatorial).

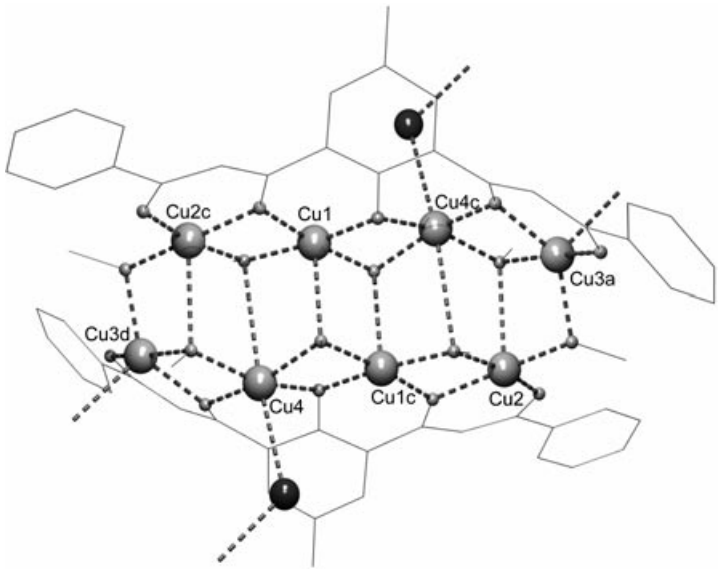

Figure 6. POV-Ray representation of the structure of the major component of $[Cu_8(L)_2(OMe)_{3.93}(Br)_{1.07}]$ (**4**). Only the Cu atoms are labeled. Cu: large gray; O: small gray; Br: medium black; C: rest. Bonds to Cu are highlighted as dashed lines. Bond length ranges [Å]: Cu–$O_{eq.}$ 1.898(2)–1.974(2); Cu–$O_{ax.}$ 2.376(2)–2.884(2); Cu–Br 2.399(6)–2.7100(4); Cu3–O2 1.997(2) (this bond is neither axial nor equatorial).

differing slightly in the exact measure of the metric parameters. Thus, the τ values of the five coordinate Cu ions are 0.06 (Cu1), 0.06 (Cu2), and 0.50 (Cu3), respectively, and the Cu-Cu-Cu angles within the tetranuclear chains are 170.59(1)° (Cu2-Cu1c-Cu4) and 155.09(1)° (Cu1c-Cu4-Cu3d), respectively. Complex **4** displays the same 1D arrangement of $[Cu_8]$ units (not shown) as **3**, this time bridged by bromide ligands with Cu-Br-Cu angles of 124.24°, with the shortest Cu···Cu intercluster distance of 4.6710(5) Å (Cu3···Cu4), thus 0.2 Å longer than in **3**. The distances between O-bridged Cu^{II} centers, however, are very similar to these in the chloride compound, and measure 2.8947(4) to 2.9904(4) Å (all O donors on equatorial positions) and 3.0010(5) to 3.5652(4) Å (some O donors on axial positions), respectively.

*$[Cu_8(L)_2(OMe)_8(ClO_4)_2(MeOH)_4]$ (**5**)*: Complex **5** is an interesting addition to the above family of $[Cu_8]$ compounds in that its structure (Figure 7) shows an octanuclear unit, similar to these of **2**, **3**, and **4**, which, in this case, is not bridged into infinite chains, but appears in the form of discrete isolated clusters. This drastic change in the spatial organization of the clusters is caused by the nature of the anionic ligand. In **5**, this ion is ClO_4^-, which acts as bidentate ligand of Cu^{II} on the $[Cu_8]$ clusters but does not facilitate intercluster linkage through coordination bonds. Another feature that is unique, within this family, to complex **5** is that four vacant coordination sites are occupied by MeOH molecules (O5, O7, and their symmetry equivalents, which, according to elemental analysis, are replaced by H_2O upon exposure to air). Thus, Cu1, Cu2, and Cu3 are in elongated octahedral coordination environments, whereas the geometry of Cu4 is closer to square pyramidal (τ = 0.35) than the

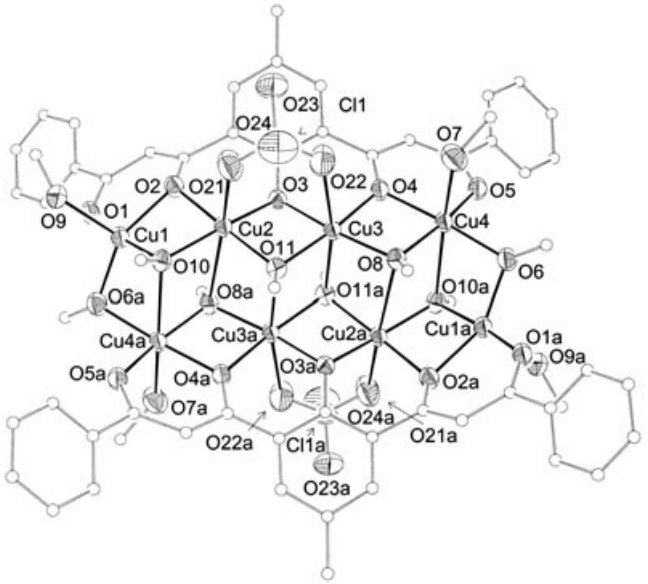

Figure 7. ORTEP representation at the 50% probability level of $[Cu_8(L)_2(OMe)_8(ClO_4)_2(MeOH)_4]$ (**5**). Carbon atoms are represented as isotropic spheres. Hydrogen atoms are not shown for clarity. Non-carbon atoms are labeled. Bond length ranges [Å]: Cu–$O_{eq.}$ 1.911(3)–1.975(3); Cu–$O_{ax.}$ 2.417(3)–2.701(3); Cu–O(MeOH), 2.346(4) and 2.368(5); Cu–O-(ClO_4), 2.349(5) and 2.500(5).

analogue ions in **2**, **3**, and **4**. The angles between metals within the tetranuclear arrays are 160.43(3)° (Cu1-Cu2-Cu3) and 171.24(3)° (Cu2-Cu3-Cu4), respectively. The distances between adjacent Cu^{II} ions are in the ranges 2.860(1) to 3.001(4) Å and 2.981(1) to 3.564(1) Å, within and across the $[Cu_4]$ moieties, respectively.

catena-$[Cu_4(L)(OMe)_3(NO_3)_2(H_2O)_{0.36}]$ (***6***): The asymmetric unit of complex **6** (Figure 8) is very similar to that of **2** (Figure 2). Again, it features four closely spaced Cu^{II} ions assembled by the chelating effect of the five adjacent oxygen atoms of the ligand L^{3-}. They only differ in the ratio of OMe^- versus NO_3^- groups, which is 3:2 in **6** compared to 4:1 in **2**. This seemingly small difference has a profound effect on the manner in which the $[Cu_4L]^{5+}$ building blocks organize into more complex architectures. In **2**, the ratio of bridging ligands is such that the aggregation of the $[Cu_4L]^{5+}$ units occurs in the form of a facial dimerization to yield octanuclear entities. In **6**, by contrast, each tetranuclear moiety is linked to two other equivalent fragments in a shifted manner, rather than face to face, which leads to an infinite succession of such motifs, intimately bridged by μ_3-OMe^- groups without discontinuity (Figure 9). There are two different ways in which the $[Cu^{II}_4L]^{5+}$ units are connected; they involve different contact lengths. The linkage of the largest contact involves a total of four μ_3-OMe^- ligands and two η^2:μ_2-NO_3^- groups. The other connection mode occurs through the action of two μ_3-OMe^- groups, one η^2:μ-NO_3^- ligand, and one η^2:μ_3-NO_3^- moiety. Contrary to compound **2**, there are no μ-OMe^- ligands in this complex. In addition to the bridging ligands already described, the asymmetric unit also contains one terminal ligand consisting of a partially occupied molecule of water (with refined occupancy of 0.362(5)) coordinated to Cu1 and H bonds donating to two NO_3^- ions (Figure 10). The presence or absence of this molecule slightly influences the orientation of the NO_3^- group bridging Cu4 to Cu2, which is therefore disordered over two

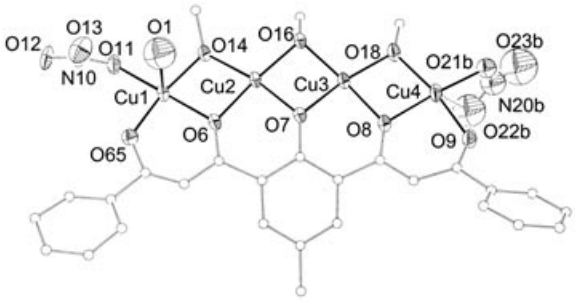

Figure 8. Representation of the asymmetric unit of the $[Cu_4(L)(OMe)_3(NO_3)_2(H_2O)]$ component of (**6**). Hydrogen atoms have been removed for clarity. Non-carbon atoms are labeled and represented as displacement ellipsoids at the 50% probability level.

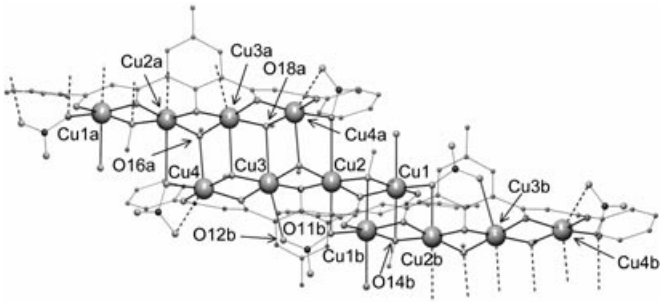

Figure 9. POV-Ray representation of the $[Cu_4(L)(OMe)_3(NO_3)_2(H_2O)]$ component of (**6**) in the crystal showing the organization of the $[Cu_4]$ oligomers into an infinite 1D coordination polymer. Cu atoms and atoms listed in Table 2 not shown in Figure 5 are labeled. Hydrogen atoms have been removed for clarity. Cu: large gray; O: medium gray; N: medium black; C: rest. The dashed lines are bonds to neighboring equivalent $[Cu_4]$ arrays.

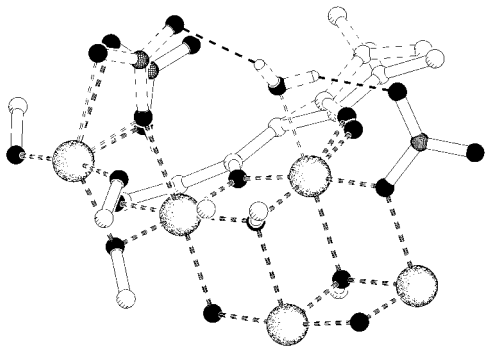

Figure 10. PLATON representation showing the partially occupied coordinated water molecule in **6**. Minor component bonds are displayed as open, dashed bonds, with exception of the hydrogen bonding. All hydrogen atoms not involved in hydrogen-bonding and all atoms located further than 6 Å from the water oxygen have been omitted for clarity. The disordered phenyl ring is therefore not complete. Cu: large; O: small black; N: small hashed; C: rest.

positions. This disorder is also present in the "Ph-C=O" moiety of L^{3-} containing the atom O5 or O65 (minor component). In both Figures 8 and 9, the minor component of the structure is represented, which contains the coordinated water molecule. The coordination around copper in complex **6** is exclusively ensured by O donors. In the repeating unit of this polymer there are two Cu^{II} centers (Cu2 and Cu3) in an octahedral coordination environment, one Cu^{II} ion (Cu1) whose coordination geometry is distributed between two types, octahedral or square pyramidal ($\tau = 0.03$) according to the disorder present in this compound (0.362(5):0.638(5)), and a fourth metal (Cu4) that can be described as square pyramidal with an additional, very long (2.710(11) or 2.522(18) Å), axial bond to a NO_3^- ligand (disordered owing to the partial presence of a coordinated water molecule, see above), which in this form is acting as a chelating anion. The metallic core of **6** is an infinite array of oligomeric units intimately linked by methoxide ligands. To the best of our knowledge, such an arrangement is unique. However, a related series of compounds with stoichiometry $Cu_nX_{2n}L_2$ (X = halide, L = halide or neutral ligand) have been prepared that feature infinite stacks of oligomeric $[Cu_n]$ fragments.[26,27] Within the coordination polymer **6** there are eight unique $[Cu_2O_2]$ pairs with the following Cu···Cu distances: 2.8502(8) to 2.9645(8) (within the $[Cu^{II}_4L]^{5+}$ unit), 3.3255(8) and 3.3766(9) Å (within the short link), and 3.2781(8) to 3.4294(8) Å (within the long link). Interestingly, in this structure the repeating arrays of four Cu^{II} metals are less bent than in compound **2**, as gauged by the Cu1-Cu2-Cu3 and Cu2-Cu3-Cu4 angles (171.22(3)° and 172.43(3)°, respectively).

Magnetochemistry: The nature of the magnetic exchange in **1**, **2**, **5**, and **6**, as representative of the different categories of complexes, was examined by susceptibility measurements. Complex **1** was investigated to assess a possible interexchange between its distant Cu^{II} centers, mediated by the HL^{2-} ligand and presumed to be very weak. Of particular interest was the study of the magnetic properties of **2**, **5**, and **6**, because both contain the same very unusual $[Cu_4L]^{5+}$ magnetic building block gathered by L^{3-}, although organized into dramatically different supramolecular structures.

Bulk magnetization measurements of the dinuclear complex $[Cu_2(HL)_2(dmf)_2]$ (**1**) were collected in the 1.8–300 K temperature range under a constant magnetic field of 500 or 10000 G. In the plot of experimental $\chi_m T$ versus T (see Figure S2 in the Supporting Information), where χ_m is the molar magnetic susceptibility per $[Cu_2]$ unit, the value of $\chi_m T$ at room temperature is 0.92 $cm^3 K mol^{-1}$, which is very close to the expected number for a molecule containing two magnetically uncoupled Cu^{II} ions ($S = 1/2$) with $g = 2.19$ (0.90 $cm^3 K mol^{-1}$). This value remains practically constant over the entire temperature range and drops suddenly at low temperatures (≈30 K) to reach 0.62 $cm^3 K mol^{-1}$ at 2 K. This behavior suggests the presence of a very weak antiferromagnetic coupling between the Cu^{II} centers that is only manifested at very low temperatures. The extent of the coupling was determined by fitting the experimental data of χ_m to the Bleaney–Bowers equation for two exchanged coupled Cu^{II} centers.[28,29] To this theoretical expression was added a temperature-independent paramagnetism (TIP) term, which was allowed to vary during the fitting procedure. The best fit (Figure S2, solid line) was obtained for values of $g = 2.19$, $J = -0.73\ cm^{-1}$ (with the $H = -2JS_1S_2$ convention for the Heisenberg Spin Hamiltonian) and TIP = $58 \times 10^{-6}\ cm^3 mol^{-1}$.

The bulk magnetization at variable temperature of $[Cu_8(L)_2(OMe)_8(NO_3)_2]$ (**2**) under a constant magnetic field was also examined. Data were collected at temperatures between 1.8 and 300 K with an applied magnetic field of 1000 G. A plot of the experimental $\chi_m T$ versus T values per $[Cu_8]$ unit corrected for temperature-independent paramagnetism (TIP = $0.48 \times 10^{-3}\ cm^3 mol^{-1}$) is represented in Figure 11 (inset). This plot has the same qualitative appearance as that originally reported,[17] but it is shifted to lower values. This is attributed to experimental error during sample preparation in the preliminary work that produced anomalously higher values of $\chi_m T$. At room temperature, the product $\chi_m T$ takes the value of 2.29 $cm^3 K mol^{-1}$, which is smaller than the expected number for eight independent Cu^{II} ions with $g = 2$ (3.00 $cm^3 K mol^{-1}$). This value drops quite rapidly with decreasing temperature to reach 0.02 $cm^3 K mol^{-1}$ at 1.8 K. These results show that the spin magnetic moments of the Cu^{II} centers are strongly coupled antiferromagnetically. This interaction is already manifested at room temperature and leads to a diamagnetic spin ground state of the $[Cu_8]$ units. The sharp raise at the lowest temperatures in the plot of χ_m versus T (Figure 11) underscores the presence of a small amount of uncoupled paramagnetic impurity (very common in this type of system and especially apparent with strongly antiferromagnetic compounds). To describe quantitatively the magnetic exchange within the cluster, the experimental data of the magnetic

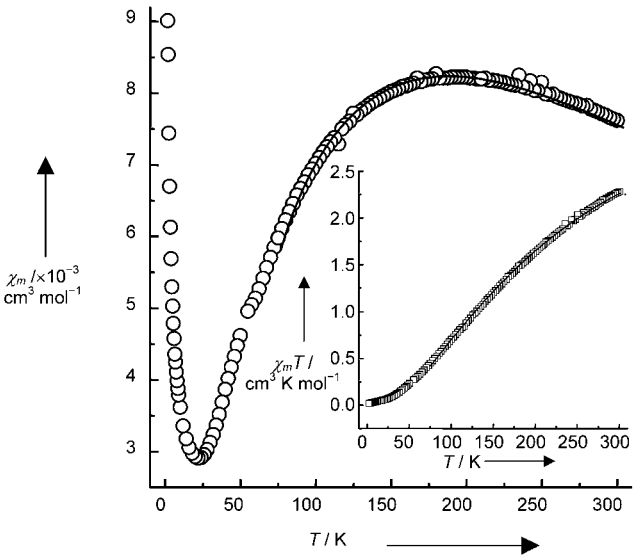

Figure 11. Plot of experimental χ_m versus T for $[Cu_8(L)_2(OMe)_8(NO_3)_2]$ (**2**) per $[Cu_8]$. The solid line is a fit to the $T > 80$ K experimental data using the program CLUMAG (see text for details). The inset is a representation of the same data plotted as $\chi_m T$ versus T.

susceptibility were fitted to a theoretical model. Figure 12 shows a scheme of the core of **2** indicating the seven independent interactions between nearest Cu ions that are necessary to describe the magnetic coupling within **2**. The spin topology of this system precludes the use of a Kambe vector coupling method to obtain the energies of the spin states. Instead, a numeric method was employed by using the program CLUMAG.[30] This program finds the set of parameters that best fits a spin-only model to the experimental data after an iterative procedure. This iteration is performed by diagonalization of the matrix resulting from the consideration of a particular coupling scheme by means of the irreducible tensor operator (ITO) formalism. To avoid over-parametrization in the calculation for compound **2**, only the interactions deemed most likely to dominate the coupling were considered. In this approximation, it was assumed that any intercluster interaction was negligible because those would be mediated by NO_3^- bridges, all through long axial bonds to Cu. Within the [Cu_8] unit, the interactions occurring through short equatorial Cu–O bonds were considered to be the most important, whereas those involving axially long or Jahn–Teller elongated bonds were estimated to be negligible. Such an approximation is especially appropriate with systems where the main interactions are antiferromagnetic, which suppress any other weaker effect that otherwise would only be apparent at lower temperatures. This resulted in the model shown in Scheme 2A, in which the crystallographic symmetry of the cluster was considered that can be described by the spin Hamiltonian of Equation (2).

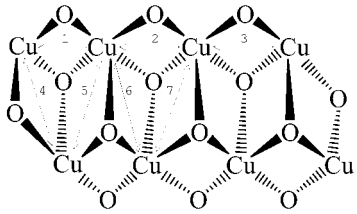

Figure 12. Schematic representation of the [Cu_8O_{14}] core of [$Cu_8(L)_2(OMe)_8(NO_3)_2$] (**2**). The arrows show the seven unique interactions between adjacent Cu ions necessary to describe the magnetic coupling within the cluster.

$$H = -2J_1(S_1S_2 + S_{1'}S_{2'}) - 2J_2(S_2S_3 + S_{2'}S_{3'}) - 2J_3(S_3S_4 + S_{3'}S_{4'}) - 2J_4(S_4S_{1'} + S_{4'}S_1) \quad (2)$$

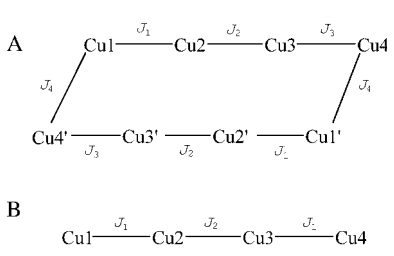

Scheme 2. Spin topologies employed to model the magnetic coupling within **2** (A) and **6** (B), respectively.

In this equation, S_i or $S_{i'}$ are the spin operators of Cu_i and $Cu_{i'}$, respectively. To limit the perturbing effects of the paramagnetic impurity during the fit, which are magnified at low temperatures because of the strong antiferromagnetic character of **2**, only the data above 80 K were included. A group of best parameters was obtained from the numeric procedure, in which nonadjacent J constants became grouped into two sets of one value each, despite being left to vary freely. These values are $J_1 = J_3 = -104\,cm^{-1}$ and $J_2 = J_4 = -90\,cm^{-1}$. An almost equally satisfactory fit (solid lines in Figure 9) was obtained when the calculation was carried out under the constraint $J_1 = J_2$, yielding the parameters $J_1 = J_2 = -99\,cm^{-1}$, $J_3 = -114\,cm^{-1}$ and $J_4 = -81\,cm^{-1}$. This was the preferred result because it bears more physical sense (vide infra) than the previous one. In these fits, an upper limit of 2.30 was imposed for the value of g. The strong antiferromagnetic coupling constants revealed by this analysis are consistent with extensive experimental and theoretical studies performed on the spin exchange within [Cu_2O_2] units constituted by hydroxide,[31] alkoxide,[32,33] or phenoxide[34] equatorial bridges. It is clear from this vast amount of research that the nature and strength of the exchange is chiefly affected by the Cu-O-Cu angle (referred to as φ below). In general, the coupling is antiferromagnetic and $|J|$ decreases as φ becomes more acute. For each type of bridge there is a predicted critical value of φ where J changes sign to become ferromagnetic. The antiferromagnetic character of the interaction is favored by the nature of the bridge in the order OPh > OR > OH. Other geometric or electronic factors have also been found to exert a particular influence on the value of J, such as the coordination geometry around Cu^{II},[35–37] the Cu–O bond distances,[38,39] or the electronegativity of the additional ligands bound to the metals.[40] All spin interactions modeled for compound **2** correspond to the above-mentioned [Cu_2O_2] categories, except for that between Cu1 and Cu4′ (and its symmetric equivalent) where only one of the two Cu-O-Cu pathways involves two short equatorial Cu–O bonds. The bridging ligands are methoxide, phenoxide, or pseudoalkoxides arising from the diketonate moieties. In all cases, the Cu-O-Cu angles are well inside the range expected for strong antiferromagnetic coupling, respectively, consistent with the results from the fit. The smallest J value (J_4, $-81\,cm^{-1}$) has been assigned to the Cu1···Cu4′ interaction (and its symmetric counterpart), since it only has one equatorial MeO^- bridge. The two degenerate intermediate coupling constants (J_1 and J_2, $-99\,cm^{-1}$) are attributed to the Cu1Cu2 and Cu2Cu3 pairs (and their respective symmetric equivalents). For these pairs, φ ranges from 94.24 to 96.27°. The strongest interaction (J_3, $-114\,cm^{-1}$) is associated with the Cu3···Cu4 coupling, which involves Cu-O-Cu angles of 99.75 and 100.96°, and is therefore expected to display enhanced antiferromagnetism. Because of the approximations included in this analysis, however, the numbers obtained must be regarded with skepticism.

For comparison, bulk magnetization measurements of the discrete octanuclear complex [$Cu_8L_2(OMe)_8(ClO_4)_2(MeOH)_4$] (**5**) were performed at temperatures between 2 and 300 K under a constant magnetic field of 1 T. The plot

of $\chi_m T$ versus T (Figure S3) is very similar to that of complex **2**. This is in agreement with the above assumption that the magnetic properties of compounds **2**–**5** are dominated by the exchange within the octanuclear core, which is very similar in all these complexes. For this reason, a numerical treatment of the experimental data was not attempted with **5**.

The variable-temperature magnetic susceptibility of *catena*-$[Cu_4(L)(OMe)_3(NO_3)_2(H_2O)_{0.36}]$ (**6**) was investigated under the influence of a constant magnetic of 1000 or 10000 G in the same temperature range as **1**, **2**, and **5**. The results, per $[Cu_4]$ unit and corrected for TIP ($0.24\times10^{-3}\,cm^{-3}mol^{-1}$), are represented in Figure 13 as χ_m or $\chi_m T$

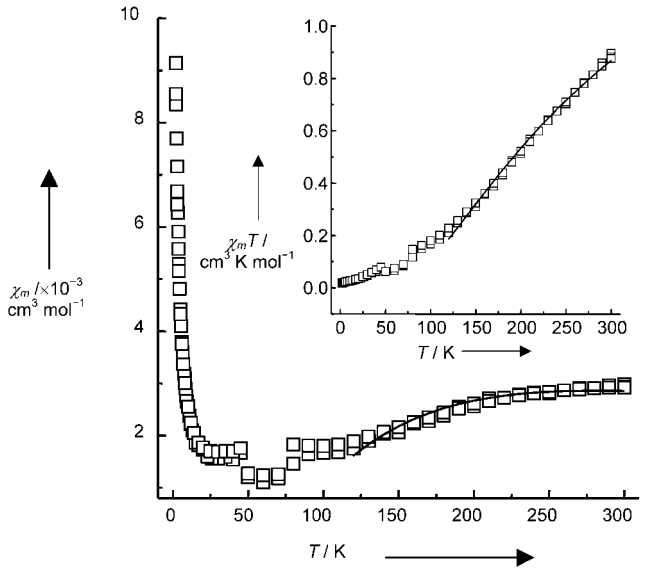

Figure 13. Plot of experimental χ_m versus T for *catena*-$[Cu_4(L)(OMe)_3(NO_3)_2(H_2O)_{0.36}]$ (**6**) per $[Cu_4]$. The solid line is a fit to the $T>120$ K experimental data using the program CLUMAG (see text for details). The inset is a representation of the same data plotted as $\chi_m T$ versus T.

(inset) vs T plots. For each representation, the plots at both magnetic fields were found to be superimposable. The $\chi_m T$ experimental curve is very similar in appearance to that of the $[Cu_8]$ cluster in **2**. The room temperature value of $\chi_m T$ per $[Cu_4]$ moiety is $0.90\,cm^3\,K\,mol^{-1}$, which is significantly smaller than that expected for four magnetically uncoupled Cu^{II} centers ($1.5\,cm^{-3}\,K\,mol^{-1}$). A decrease is observed as the sample is cooled, until a value of $0.02\,cm^3\,K\,mol^{-1}$ is reached at 1.8 K. This behavior reveals that very strong antiferromagnetic interactions dominate the magnetic coupling within this system. As a result, a small amount of a paramagnetic impurity becomes very apparent in the χ_m versus T plot at the lowest temperature range ($\approx$20 to 2 K). The strong antiferromagnetic character of the coupling in this sample results in the extreme weakness of the signal in the approximate range between 25 and 100 K, causing the data in this interval to be subject to an important experimental error. Thus, only data above 120 K were used for its quantitative description. For this, the experimental data in that interval was fit with the program CLUMAG as before. Again, it was considered that the magnetization in **6** was controlled by the interactions within equatorially bridged $[Cu_2O_2]$ moieties. Therefore, the coupling between metal ions in different $[Cu_4]$ units, occurring through axial Jahn–Teller elongated bonds, was assumed to be suppressed by the strong antiferromagnetic exchange prevailing within the tetranuclear chains. Thus, a $2J$ model was used (Scheme 2B) consisting of independent arrays of four Cu^{II} ions bridged by L^{3-}, as described by the spin Hamiltonian $H = -2J_1(S_1S_2+S_3S_4)-2J_2(S_2S_3)$. The symmetry imposed in this model within the $[Cu_4]$ arrays is a consequence of the similarity in structural parameters of the Cu1Cu2 and Cu3Cu4 pairs (range of Cu-O-Cu angles: 99.16 to 101.24°) in contrast with the Cu2Cu3 pair (Cu-O-Cu angles: 93.83 and 94.97°). The best fit was obtained for $J_1 = -177$ and $J_2 = -154\,cm^{-1}$, with an imposed maximum for g of 2.30. These values may only be taken as indicative on account of the number of approximations invoked and the weakness of the signal. It was found, however, that the quality of the fit was little affected by the value of the central interaction, provided it remained less antiferromagnetic than J_1. This dominance of the coupling by two external antiferromagnetic interactions over an innocent central exchange has already been observed in other Cu_4 systems with the same spin topology.[41] The Hamiltonian adopted here to model the experimental data of **6** can not be solved by the Kambe vector coupling method[42] but has an analytical solution, as reported previously for a Cu_4 complex with the same symmetry.[41] Therefore, the data was fitted to the equation given in reference [42] to give the following parameters: $J_1 = -166$ and $J_2 = -142\,cm^{-1}$, whereby an upper limit of 2.3 for g was imposed. Again, this fit is not affected significantly by the value of J_2, provided it remains less antiferromagnetic than J_1. If the approximations used are kept in mind, as well as the inaccuracy derived from the low intensity of the magnetization in this system, the results arising from both fits are comparable. The extent of the exchange, however, seems to be significantly stronger in this complex than in **2**. The structural differences of these two compounds prevent a systematic comparison between their J values. However, the strongest interaction, which controls the coupling in both cases, can be compared. In both compounds, the corresponding Cu···Cu pair features the largest Cu-O-Cu angles, which are similar for both compounds (average of 100.4 and 100.3° in **2** and **6**, respectively). Among the factors causing this interaction to be stronger in **6** could be the fact that in this complex the Cu–O distances are slightly shorter (average of 1.940 versus 1.953 Å),[38,39] or that it displays a smaller hinge distortion of the $[Cu_2O_2]$ moiety (Cu-O-O-Cu torsion angles of 172.9 and 171.2° in **6** vs 168.6° in **2**), which has been shown to have an important effect on the nature of the magnetic exchange.[38,39,43,44]

Conclusions

Herein, the great potential of the H_3L ligand for the aggregation of Cu^{II} spin carriers into structures with different degrees of aggregation and magnetic spin–spin interactions has been shown. The identity of the product formed can be

chemically controlled by small changes in the reaction conditions. A binuclear complex with very weakly interacting Cu^{II} ions is formed when the stoichiometric amount of a mild base is used. In contrast, full deprotonation of H_3L is achieved by the use of an excess of a stronger base, which leads to the assembly of tetranuclear arrays of closely spaced and strongly interacting Cu^{II} ions. This structural moiety is attained exclusively as a result of the templating capability of L^{3-} which is based on its five strategically positioned O donors. Subtle variations in the stoichiometry lead to a dramatic change in the supramolecular organization of the $[Cu^{II}_4]$ magnetic building blocks, starting from arrays of $[Cu_4]_2$ units and changing to a chain of strongly linked $[Cu_4]$ oligomers. The supramolecular organization of the octanuclear $[Cu_4]_2$ entities can be influenced by the nature of the accompanying counterion. Thus, infinite chains of clusters are formed as a result of the bridging action of NO_3^-, Cl^-, or Br^-, whereas the use of ClO_4^- blocks the polymerization and leads to the formation of independent $[Cu_4]_2$ cages. This work is therefore an important contribution towards the goal of exploiting chemical tools in the construction of molecular-based magnetic materials with complicated structures and tunable magnetic properties. Extension of this chemistry to other open-shell transition metals is currently underway.

Experimental Section

Physical measurements: IR spectra were collected on a Perkin-Elmer Paragon 1000 spectrophotometer equipped with a Golden Gate Diamond ATR as a sample support. Bulk magnetization measurements of smoothly powdered microcrystalline samples of (**1**, 24.7 mg), (**2**, 18.1 mg), (**5**, 3.8 mg), and (**6**, 15.0 mg) were performed in the range 300–1.8 K with a Quantum Design MPMS-XL (**1** and **6**) or MPMS-7XL (**2** and **5**) SQUID magnetometer with an applied field of 0.5, 1, or 10 kG. Data were corrected for the magnetization of the sample holder. Diamagnetic contributions were calculated using Pascal's constants (-5.12, -6.14, -7.46, and -2.86×10^{-4} $cm^3 K mol^{-1}$ for **1**, **2**, **5**, and **6**, respectively). Elemental analyses were performed in-house on a Perkin Elmer Series II CHNS/O Analyzer 2400, at the Servei de Microanàlisi of CSIC, Barcelona (Spain), or at the Microanalytical Laboratory of the University College, Dublin (Ireland).

Syntheses: All reagents were used as received except if otherwise indicated. The ligand H_3L (1,3-bis(3-oxo-3-phenylpropionyl)-2-hydroxymethylbenzene) was prepared according to a previously published procedure.[12]

$[Cu_2(L)_2(dmf)_2]$ (1): To a blue solution of $Cu(AcO)_2{\cdot}H_2O$ (25 mg, 0.13 mmol) in DMF (5 mL) was added a yellow solution of H_3L (50 mg, 0.13 mmol) in DMF. The solution turned dark green. It was stirred for a few minutes and was then left unperturbed at -5 °C overnight. Crystals of **1** were then collected by filtration. Yield: 47%; elemental analysis calcd (%) for $C_{63.2}H_{66.8}N_{4.4}Cu_2O_{14.4}$ (**1**·2.4 DMF, 1046.11): C 60.94, H 5.41, N 4.95; found: C 60.56, H 5.26, N 4.61.

$[Cu_8(L)_2(OMe)_8(NO_3)_2]$ (2): To a blue solution of $Cu(NO_3)_2{\cdot}2.5H_2O$ (233 mg, 1 mmol) in MeOH (14 mL) was added dropwise an orange solution of H_3L (50 mg, 0.13 mmol) and nBu_4NOH (1.8 mL of a 1 M solution in MeOH, 1.8 mmol) in MeOH (14 mL). The solution turned dark green and a fine green precipitate started to form before the addition was complete. The mixture was stirred for about 30 min, and the precipitate was collected by filtration. The green solid was immediately slurried in MeOH for about 30 min and then separated by filtration. The remaining green-yellow filtrate was layered with Et_2O in various tubes and left for 2 weeks, after which, green crystals of **2**, suitable for X-ray crystallography, had been deposited on the sides and were collected by filtration. Yield: 20%; elemental analysis calcd (%) for $C_{59}H_{62}N_2Cu_8O_{25}$ (**2**·MeOH, 1707.56): C 41.50, H 3.66, N 1.64; found: C 41.11, H 3.30, N 1.75.

Complex **2** was found to decompose upon exposure to air. Therefore, when the solid was separated from the mother liquor, it was manipulated in a glove box and all the physical measurements were performed under an inert atmosphere. Microanalysis experiments suggest that complex **2** undergoes complete substitution of the OMe^- ligands by OH^- in contact with atmospheric moisture to form the fully hydrolyzed product $[Cu_8(L)_2(OH)_8(NO_3)_2]$ (**2a**). Elemental analysis calcd (%) for $C_{50}H_{46}N_2Cu_8O_{26}$ (**2a**·2 H_2O, 1599.32): C 37.55, H 2.90, N 1.75; found: C 37.14, H 2.42, N 1.92.

$[Cu_8(L)_2(OMe)_8(Cl)_2]$ (3): This complex was prepared in the same manner as complex **2** from $CuCl_2{\cdot}2H_2O$ (170.45 mg, 1 mmol) instead of the nitrate salt, and was obtained as green crystals, suitable for X-ray crystallography, in similar yields. The compound absorbs H_2O upon exposure to air. Elemental analysis calcd (%) for $C_{58}H_{70}Cl_2Cu_8O_{24}$ (**3**·6 H_2O, 1730.5): C 40.26, H 4.08; found: C 39.89, H 3.31.

$[Cu_8(L)_2(OMe)_{7.86}Br_{2.14}]$ (4): This compound was prepared in the same manner as complexes **2** and **3** from $CuBr_2$ (223.36 mg, 1 mmol) as the Cu^{II} salt. Green crystals were obtained in ≈20% yield. They were used for single-crystal X-ray diffraction studies. The compound absorbs H_2O upon exposure to air. Elemental analysis calcd (%) for $C_{57.86}H_{65.58}Br_{2.14}Cu_8O_{21.86}$ (**4**·4 H_2O, 1790.2): C 38.82, H 3.69; found: C 38.51, H 3.35.

$[Cu_8(L)_2(OMe)_8(ClO_4)_2(MeOH)_4]$ (5): This complex was prepared as for **2**, **3**, and **4**, from $Cu(ClO_4)_2{\cdot}6H_2O$ as the metal salt but with different stoichiometries. Thus a solution of $Cu(ClO_4)_2{\cdot}6H_2O$ (370 mg, 1 mmol) in MeOH (15 mL) was mixed with another solution of H_3L (100 mg, 0.25 mmol) and nBu_4NOH (1.8 mL of a 1 M solution in MeOH, 1.8 mmol) in MeOH (14 mL). The resulting green slurry was treated in the same manner as in the above three preparations. Extremely thin plates were obtained in yields of 10–15%. The terminal MeOH was replaced by H_2O upon exposure to air to form $[Cu_8(L)_2(OMe)_8(ClO_4)_2(H_2O)_4]$ (**5a**). Elemental analysis calcd (%) for $C_{58}H_{66}Cl_2Cu_8O_{30}$ (**5a**, 1822.46): C 38.23, H 3.65; found: C 37.65, H 3.30.

***catena*-$[Cu_4(L)(OMe)_3(NO_3)_2(H_2O)_{0.36}]$ (6)**: To a stirred blue solution of $Cu(NO_3)_2{\cdot}2.5H_2O$ (349 mg, 1.5 mmol) in MeOH (45 mL) was added an orange solution of H_3L (150 mg, 0.38 mmol) and nBu_4NOH (1.5 mL of a 1 M solution in MeOH, 1.5 mmol) in MeOH (45 mL). The solution turned dark green, and stirring was maintained for about 20 min. The system was left unperturbed after addition of Et_2O (100 mL), and 3 weeks later, small black needles of **6**, which were suitable for X-ray diffraction, were collected in 25% yield. Elemental analysis calcd (%) for $C_{28}H_{26.8}N_2Cu_4O_{14.4}$ (**6**·0.04 H_2O, 875.93): C 38.39, H 3.08, N 3.20; found: C 38.20, H 3.21, N 3.19.

X-ray crystallography:

*Complexes **1** and **2***: Details of the crystal structure determination of complexes **1** and **2** have been published elsewhere.[17,20]

*Complex **3***: $C_{58}H_{52}Cl_2Cu_8O_{18}{\cdot}1.5\,CH_3CH_2OCH_2CH_3$, $M_r = 1727.40$, green block, triclinic, space group $P\bar{1}$ with $a = 10.640(4)$, $b = 13.525(5)$, $c = 13.566(4)$ Å, $\alpha = 101.278(5)$, $\beta = 101.278(5)$, $\gamma = 96.568(4)$°, $V = 1850.8(11)$ Å^3, $Z = 1$, $\rho_{calcd} = 1.550$ g cm^{-3}, $F(000) = 873$, $\mu(Mo_{K\alpha}) = 2.389$ mm^{-1}. X-ray data were collected on a Bruker SMART CCD area-detector single-crystal diffractometer with graphite-monochromatized $Mo_{K\alpha}$ radiation ($\lambda = 0.71073$ Å) by the ϕ–ω scan method at 293 K. A total of 11980 reflections were measured ($1.57 < \theta < 28.30$°), 8420 of which were independent ($R_{int} = 0.0392$). The structure was solved by direct methods using the program SHELXS-97.[45] The refinement and all further calculations were carried out using SHELXL-97.[46] The H atoms could be located from Fourier difference maps but were finally treated as riding atoms using SHELXL default parameters. The non-hydrogen atoms were refined anisotropically with weighted full-matrix least-squares on F^2. A region of highly disordered electron density was equated to 1.5 molecules of diethyl ether per molecule of complex and the HKL file was modified with the SQUEEZE routine in PLATON;[47] 66 electrons for a volume of 513 Å^3. Refinement of 392 parameters resulted in a final $wR2$ of 0.1075, $w = 1/[\sigma^2(F^2) + (0.0506P)^2]$, where $P = (\max(F_o^2,0) + 2F_c^2)/3$, $R1 = 0.0514$ (for 4713 $I > 2\sigma(I)$), $S = 0.893$, $-0.628 < \Delta\rho < 0.659$ e Å^{-3}.

*Complex **4***: $C_{57.86}H_{57.58}Br_{2.14}Cu_8O_{17.86}{\cdot}CH_3CH_2OCH_2CH_3$, $M_r = 1792.15$, green block, ($0.40 \times 0.27 \times 0.33$ mm), triclinic, space group $P\bar{1}$ with $a = 10.7644(7)$, $b = 13.6003(9)$, $c = 13.4636(9)$ Å, $\alpha = 101.250(5)$, $\beta =$

109.288(5), γ = 101.549(5)°, V = 1869.3(2) Å^3, Z = 1, ρ_{calcd} = 1.592 g cm^{-3}, $F(000)$ = 897, $\mu(Mo_{K\alpha})$ = 3.435 mm^{-1}. The intensity data were collected at 153 K on a Stoe Mark II Image Plate Diffraction System equipped with a two-circle goniometer with $Mo_{K\alpha}$ graphite-monochromated radiation (λ = 0.71073 Å). A total of 20740 reflections were measured ($1.14 < \theta < 29.77°$), 9748 of which were independent (R_{int} = 0.0301). The structure was solved by direct methods using the program SHELXS-97.[45] The refinement and all further calculations were carried out using SHELXL-97.[46] An empirical absorption correction with DIFABS in PLATON was applied; transmission factors T_{min}/T_{max} = 0.311/0.747. The SQUEEZE routine in PLATON was also applied and gave a solvent area occupied by ≈40 electrons for a volume of 509.5 Å^3. This was equated to one molecule of diethyl ether per unit cell (per $[Cu_8]$ complex molecule). A peak in the region of the methoxy group bridging atoms Cu2 and Cu3 was assumed to be a partially occupied bromine atom, whereby bond lengths were used as a reference. The refined occupancies for the CH_3O/bromine were 0.931/0.069. Hence, we can assume that atoms Cu2 and Cu3 are bridged by a Br for ≈7% of the molecules in the crystal, and atoms Cu2 and Cu3 are bridged by a methoxy group for ≈93% of the molecules in the crystal. The hydrogen atoms were included in calculated positions as riding atoms using SHELXL default parameters. Non-hydrogen atoms were refined anisotropically with weighted full-matrix least-squares on F^2. Refinement of 403 parameters resulted in a final $wR2$ of 0.0789, $w = 1/[\sigma^2(F^2)+(0.0552P)^2]$, where $P = (\max(F_o^2,0) + 2F_c^2)/3$, $R1$ = 0.0298 (for 8202 $I > 2\sigma(I)$), S = 1.003, $-0.976 < \Delta\rho < 0.724$ e Å^{-3}.

Complex ***5***: $C_{128}H_{140}Cl_4Cu_{16}O_{64}$, Fw = 3860.84, pale green plate, (0.12 × 0.06 × 0.01 mm), monoclinic, space group $P2_1/n$ with a = 15.248(2), b = 15.322(2), c = 16.244(2) Å, α = 90, β = 105.751(2), γ = 90(5)°, V = 3652.6(8) Å^3, Z = 1, ρ_{calcd} = 1.755 g cm^{-3}, $F(000)$ = 1776, μ = 2.443 mm^{-1}. The structure was determined at the microcrystal diffraction facility on station 9.8 of the Synchrotron Radiation Source, CCLRC Daresbury Laboratory. The intensity data were collected at 150(2) K on a Bruker Nonius APEX II CCD area-detector diffractometer equipped with a Cryostream nitrogen gas stream. The wavelength was calibrated by measurement of the unit cell parameters of a standard crystal of known structure. Data collection nominally covered a sphere of reciprocal space by three series of ω-rotation exposure frames with different crystal orientation ϕ angles. Reflection intensities were integrated by using standard procedures,[48] allowing for the plane-polarized nature of the primary synchrotron beam. Corrections were applied semiempirically for absorption and incident beam decay.[48] Unit cell parameters were refined from the observed ω angles of all strong reflections in the complete data sets. A total of 28330 reflections were measured ($2.541 < \theta < 25.674°$), 6963 of which were independent (R_{int} = 0.0495). The structure was solved by routine automatic direct methods and refined by least-squares refinement on all unique measured F^2 values.[49] All non-hydrogen atoms were refined anisotropically. Hydrogen atoms were found by a combination of methods: the methyl hydrogen atoms were located in the difference map and the others were placed geometrically. All were refined with a riding model. The crystal used for data collection was twinned; however, a suitable twin law could not be determined. Instead, the most disagreeable reflections were omitted from the refinement. Refinement of 485 parameters resulted in a final $wR2$ of 0.1392, $w = 1/[\sigma^2(F_o^2)+(0.0962P)^2]$, where $P = (F_o^2 + 2F_c^2)/3$, $R1$ = 0.0545 (for 5379 $I > 2\sigma(I)$), S = 1.037, $-0.654 < \Delta\rho < 1.904$ e Å^{-3}.

Complex ***6***: $0.638\,(C_{28}H_{26}Cu_4N_2O_{14})\cdot 0.362\,(C_{28}H_{28}Cu_4N_2O_{15})$, M_r = 875.23, dark green prism, (0.1 × 0.1 × 0.3 mm), monoclinic, space group $P2_1/c$ (no. 14) with a = 13.1111(10), b = 17.437(2), c = 17.271(2) Å, β = 109.288(10)°, V = 3726.8(7) Å^3, Z = 4, ρ_{calcd} = 1.560 g cm^{-3}, $F(000)$ = 1758, $\mu(Mo_{K\alpha})$ = 2.315 mm^{-1}. Data were collected at T = 150 K on an Enraf-Nonius Kappa CCD area detector on a rotating anode ($Mo_{K\alpha}$ radiation, graphite monochromator, λ = 0.71073 Å). A total of 48291 reflections were measured ($1.0 < \theta < 25.25°$), 6756 of which were independent (R_{int} = 0.0708). The structure was solved by direct methods with SHELXS86,[50] and refined on F^2 with SHELXL-97.[51] One of the Cu^{II} ions is coordinated by a partly occupied water molecule. Introduction of the water molecule causes a small shift in the position of two coordinated nitrate ions and a section of the L^{3-} ligand, compared to the situation where the water is absent. This disorder could be satisfactorily modeled with a two-site disorder model. The occupancy of the major component refined to 0.638(5). The coordinated water is only present in the minor disorder component. The crystal structure of complex **6** also contains two symmetry-related cavities with a volume of 405 Å^3 each, filled with disordered solvent. The disordered section of the L^{3-} ligand lies directly against the disordered solvent cavity. Since no satisfactory disorder model could be found, the contribution of the solvent to the structure factors was taken into account with PLATON/SQUEEZE.[47] A total of 178 electrons were found in each cavity. All hydrogen atoms of **6** were included in the refinement on calculated positions riding on their carrier atoms. Ordered non-hydrogen atoms were refined with anisotropic displacement parameters. The disordered atoms were refined with isotropic displacement parameters; the parameters for the major and minor site of each atom were equated. Hydrogen atoms were refined with a fixed isotropic displacement parameter linked to the value of the equivalent isotropic displacement parameter of their carrier atoms. Refinement of 419 parameters resulted in a final $wR2$ of 0.1122, $w = 1/[\sigma^2(F^2) + (0.0501P)^2 + 5.48P]$, where $P = (\max(F_o^2,0) + 2F_c^2)/3$, $R1$ = 0.0448 (for 5209 $I > 2\sigma(I)$), S = 1.061, $-0.80 < \Delta\rho < 0.91$ e Å^{-3}.

CCDC-225813, and CCDC-243258–243260 contain the supplementary crystallographic data for this paper. These data can be obtained free of charge via www.ccdc.cam.ac.uk/conts/retrieving.html (or from the Cambridge Crystallographic Data Centre, 12 Union Road, Cambridge CB2 1EZ, UK; fax: (+44) 1223-336033; or deposit@ccdc.cam.uk).

Acknowledgement

The authors are very grateful to the Spanish Ministerio de Ciencia y Tecnología for a "Ramón y Cajal" contract, to the Dutch WFMO (Werkgroep Fundamenteel-Materialen Onderzoek) CW (Foundation for the Chemical Sciences) and NWO (Organization for the Scientific Research), to the French CNRS (Centre National de la Recherche Scientifique), to the Conseil Général d'Aquitaine, to the European Union for the contract HPMF-CT-1999–00113 (Marie Curie Fellowship), and for the provision of time on the Small Molecule Crystallography Service at the CCLRC Daresbury Laboratory (Framework 6 program) as well as to the Swiss National Science Foundation for financial support.

[1] G. Christou, D. Gatteschi, D. N. Hendrickson, R. Sessoli, *MRS Bull.* **2000**, *25*, 66.
[2] R. Sessoli, H. L. Tsai, A. R. Schake, S. Y. Wang, J. B. Vincent, K. Folting, D. Gatteschi, G. Christou, D. N. Hendrickson, *J. Am. Chem. Soc.* **1993**, *115*, 1804.
[3] R. Sessoli, D. Gatteschi, A. Caneschi, M. A. Novak, *Nature* **1993**, *365*, 141.
[4] G. Aromí, S. M. J. Aubin, M. A. Bolcar, G. Christou, H. J. Eppley, K. Folting, D. N. Hendrickson, J. C. Huffman, R. C. Squire, H. L. Tsai, S. Wang, M. W. Wemple, *Polyhedron* **1998**, *17*, 3005.
[5] C. Cadiou, M. Murrie, C. Paulsen, V. Villar, W. Wernsdorfer, R. E. P. Winpenny, *Chem. Commun.* **2001**, 2666.
[6] D. Gatteschi, R. Sessoli, A. Cornia, *Chem. Commun.* **2000**, 725.
[7] J. R. Friedman, M. P. Sarachik, J. Tejada, J. Maciejewski, R. Ziolo, *J. Appl. Phys.* **1996**, *79*, 6031.
[8] D. Gatteschi, R. Sessoli, *Angew. Chem.* **2003**, *115*, 278; *Angew. Chem. Int. Ed.* **2003**, *42*, 268.
[9] R. E. P. Winpenny, *J. Chem. Soc. Dalton Trans.* **2002**, 1.
[10] M. Fujita, K. Umemoto, M. Yoshizawa, N. Fujita, T. Kusukawa, K. Biradha, *Chem. Commun.* **2001**, 509.
[11] V. Marvaud, C. Decroix, A. Scuiller, C. Guyardduhayon, J. Vaissermann, F. Gonnet, M. Verdaguer, *Chem. Eur. J.* **2003**, *9*, 1677.
[12] G. Aromí, P. Gamez, P. C. Berzal, W. L. Driessen, J. Reedijk, *Synth. Commun.* **2003**, *33*, 11.
[13] S. M. Peng, C. C. Wang, Y. L. Jang, Y. H. Chen, F. Y. Li, C. Y. Mou, M. K. Leung, *J. Magn. Magn. Mater.* **2000**, *209*, 80.
[14] F. A. Cotton, L. M. Daniels, C. A. Murillo, X. P. Wang, *Chem. Commun.* **1998**, 39.

[15] C. J. Matthews, S. T. Onions, G. Morata, L. J. Davis, S. L. Heath, D. J. Price, *Angew. Chem.* **2003**, *115*, 3274; *Angew. Chem. Int. Ed.* **2003**, *42*, 3166.
[16] G. Aromí, P. C. Berzal, P. Gamez, O. Roubeau, H. Kooijman, A. L. Spek, W. L. Driessen, J. Reedijk, *Angew. Chem.* **2001**, *113*, 3552; *Angew. Chem. Int. Ed.* **2001**, *40*, 3444.
[17] G. Aromí, P. Gamez, O. Roubeau, H. Kooijman, A. L. Spek, W. L. Driessen, J. Reedijk, *Angew. Chem.* **2002**, *114*, 1216; *Angew. Chem. Int. Ed.* **2002**, *41*, 1168.
[18] G. Aromí, P. Gamez, O. Roubeau, P. Carreroberzal, H. Kooijman, A. L. Spek, W. L. Driessen, J. Reedijk, *Eur. J. Inorg. Chem.* **2002**, 1046.
[19] G. Aromí, P. Gamez, O. Roubeau, P. C. Berzal, H. Kooijman, A. L. Spek, W. L. Driessen, J. Reedijk, *Inorg. Chem.* **2002**, *41*, 3673.
[20] H. Kooijman, A. L. Spek, G. Aromí, P. Gamez, P. Carrero-Berzal, W. L. Driessen, J. Reedijk, *Acta Crystallogr. Sect. E* **2002**, *E58*, m223.
[21] A. W. Addison, T. N. Rao, J. Reedijk, J. van Rijn, G. C. Verschoor, *J. Chem. Soc. Dalton Trans.* **1984**, 1349.
[22] F. B. Hulsbergen, J. Reedijk, A. L. Spek, R. W. M. Tenhoedt, G. C. Verschoor, *J. Chem. Soc. Dalton Trans.* **1983**, 539.
[23] H. W. Hou, Y. T. Fan, C. X. Du, Y. Zhu, W. L. Wang, X. Q. Xin, M. K. M. Low, W. Ji, H. G. Ang, *Chem. Commun.* **1999**, 647.
[24] J. Tercero, C. Díaz, M. S. El Fallah, J. Ribas, X. Solans, M. A. Maestro, J. Mahia, *Inorg. Chem.* **2001**, *40*, 3077.
[25] L.-Y. Wang, S. Igarashi, Y. Yukawa, Y. Hoshino, O. Roubeau, G. Aromí, R. E. P. Winpenny, *Dalton Trans.* **2003**, 2318.
[26] K. E. Halvorson, T. Grigereit, R. D. Willett, *Inorg. Chem.* **1987**, *26*, 1716.
[27] M. R. Bond, H. Place, Z. Wang, R. D. Willett, Y. Liu, T. E. Grigereit, J. E. Drumheller, G. F. Tuthill, *Inorg. Chem.* **1995**, *34*, 3134.
[28] B. Bleany, K. D. Bowers, *Proc. R. Soc. London Ser. A* **1952**, *214*, 451.
[29] O. Kahn, in *Molecular Magnetism*, VCH, New York, **1993**.
[30] D. Gatteschi, L. Pardi, *Gazz. Chim. Ital.* **1993**, *123*, 231.
[31] V. H. Crawford, H. V. Richardson, J. R. Wason, D. J. Hodgson, W. E. Hatfield, *Inorg. Chem.* **1976**, *15*, 2107.
[32] L. Merz, W. Haase, *J. Chem. Soc. Dalton Trans.* **1980**, 875.
[33] M. Handa, N. Koga, S. Kida, *Bull. Chem. Soc. Jpn.* **1988**, *61*, 3853.
[34] L. K. Thompson, S. K. Mandal, S. S. Tandon, J. N. Bridson, M. K. Park, *Inorg. Chem.* **1996**, *35*, 3117.
[35] P. J. Hay, J. C. Thibault, R. Hoffman, *J. Am. Chem. Soc.* **1975**, *97*, 4884.
[36] R. J. Butcher, E. Sinn, *Inorg. Chem.* **1976**, *15*, 1604.
[37] L. Walz, W. Haase, H. Paulus, *J. Chem. Soc. Dalton Trans.* **1985**, 913.
[38] E. Ruiz, P. Alemany, S. Alvarez, J. Cano, *Inorg. Chem.* **1997**, *36*, 3683.
[39] E. Ruiz, P. Alemany, S. Alvarez, J. Cano, *J. Am. Chem. Soc.* **1997**, *119*, 1297.
[40] H. Astheimer, W. Haase, *J. Chem. Phys.* **1986**, *85*, 1427.
[41] H. Grove, J. Sletten, M. Julve, F. Lloret, *J. Chem. Soc. Dalton Trans.* **2001**, 1029.
[42] K. Kambe, *J. Phys. Soc. Jpn.* **1950**, *5*, 48.
[43] M. F. Charlot, S. Jeannin, Y. Jeannin, O. Kahn, *Inorg. Chem.* **1980**, *19*, 1410.
[44] C. Blanchet-Boiteux, *J. Phys. Chem. A* **2000**, *104*, 2091.
[45] G. M. Sheldrick, *Acta Crystallogr. Sect. A* **1990**, *46*, 467.
[46] G. M. Sheldrick, University of Göttingen (Germany), **1999**.
[47] A. L. Spek, *J. Appl. Crystallogr.* **2003**, *36*, 7.
[48] Version 7.06a ed., Bruker AXS Inc., Madison, Wisconsin (USA), **2004**.
[49] G. M. Sheldrick, version 5.10 ed., Bruker AXS Inc., Madison, Wisconsin (USA), **1998**.
[50] G. M. Sheldrick, University of Göttingen (Germany), **1986**.
[51] G. M. Sheldrick, University of Göttingen (Germany), **1997**.

Received: July 5, 2004
Published online: November 10, 2004